Homogeneous nucleation and growth in the critical three-dimensional Ising regime of a binary polymer blend

G. Müller, D. Schwahn, and T. Springer
Forschungszentrum Jülich GmbH, Institut für Festkörperforschung, D-52425 Jülich, Germany
(Received 7 November 1996)

Phase separation in a binary blend of deutero-polystyrene and polyphenylmethylsiloxane was studied with time-resolved light scattering (small-angle light scattering) for a nearly critical concentration at temperatures between 0.2 and 2.6 K below the *binodal*. It was shown by additional neutron small-angle scattering experiments that all quenches end in the *metastable region*, i.e., in the gap between binodal and spinodal of $T_B - T_S \cong 4$ K. A Ginzburg number of 0.48 ± 0.14 was found much larger than in simple binary mixtures, indicating that thermal concentration fluctuations are very strong and that the three-dimensional (3D) Ising model is valid. It was shown that strong thermal concentration fluctuations determine the phase separation, leading to homogeneous nucleation and growth in the metastable region as proposed by Binder [Phys. Rev. A **29**, 341 (1984)]. Scattering patterns similar to those of spinodally decomposed structures were observed in a time region of the intermediate and the late stage. Power laws were obtained for the time dependence of position $Q_m(t)$ and intensity $I_m(t)$ of the scattering maximum in the late stage. Furthermore, the data were analyzed with scaling concepts based on the evolution of *self-similar* structures. The time-dependent structure factor scales in the range of $x = Q/Q_m \leqslant 2$ for all times in the late stage and all temperatures studied, following the relation $S(Q,t) = Q_m(t)^{-d} F(x)$. But instead of the Euclidean dimension $d = 3$, an exponent of $d_f = 2.43 \pm 0.05$ was found. This is tentatively explained by a precipitation process where the compactness of the domains decreases with time. In the range $x > 2$ a second characteristic length was observed, namely, an *apparent* interface thickness $l_I = 7000 \pm 200$ Å independent of time and quench depth. This was interpreted by a waviness of the interface separating the coarsening domains. Furthermore, scaling was also observed for the position $Q_m(t)$ and intensity $I_m(t)$ of the scattering maximum with the appropriate values for the collective diffusion coefficient and the correlation length in the two-phase region. Their values were determined by photon correlation spectroscopy (PCS) and small-angle neutron scattering in the one-phase region by an extrapolation into the two-phase region. Finally, by the PCS measurements an extra relaxation process with a characteristic time from 0.1 to 1 sec was discovered, which was related to density fluctuations. [S1063-651X(97)08606-6]

PACS number(s): 64.70.Ja, 64.60.Fr, 36.20.−r

I. INTRODUCTION

The investigation of phase diagrams and demixing kinetics in polymer blends has attracted great scientific interest in theory and experiment [1–4]. Polymer blends have many features in common with other systems such as metallic alloys or mixtures of simple liquids, but they reveal typical qualitative differences. Like many mixtures, polymer blends have a miscibility gap, where the binodal separates the homogeneous from the metastable and unstable regime. Approaching the critical temperature T_c on top of the miscibility gap, strong concentration fluctuations appear. One of the interesting features of these fluctuations was the observation that they follow the mean-field approximation far from T_c [5], whereas close to T_c a transition to a three-dimensional (3D) Ising behavior appears [6,7]. The transition regime and the limiting cases of mean-field and Ising behavior are covered by a general crossover function [8]. The transition temperature T^* is characterized by the so-called Ginzburg number Gi [9,10]. $\mathrm{Gi} = \epsilon^* \equiv |T^* - T_c|/T^*$ depends on the degree of polymerization N, but also on the packing density or more generally on the entropic part of the Flory-Huggins parameter [11].

The investigation of the demixing of polymer blends is especially convenient, since the corresponding characteristic times can be controlled in a wide range by the degree of polymerization. According to the mean-field theory there exist different separation processes in the two-phase regime [see Fig. 1(a)]: in the metastable region, demixing occurs by nucleation and growth; an energy barrier has to be overcome by the formation of droplets, which coarsen at later times. In the unstable region, phase separation is governed by spinodal decomposition. This process is characterized by unstable concentration fluctuations with wavelengths above a critical value. In its early stage, as long as fluctuations are small and not interacting, they can be described by a generalization of the Cahn-Hilliard-Cook theory [12,13]. Its predictions were confirmed by many experiments, with typical features related to the macroscopic chain structure, such as a nonlocal Onsager coefficient [14], or the contribution of internal modes of diffusion [15]. So far, for later stages of demixing the situation is not well understood and many aspects are still unexplained [4]. A scattering maximum appears that shifts to smaller Q values with increasing intensity [$Q = 4\pi \sin(\theta/2)/\lambda$ with scattering angle θ and wavelength of light or neutron λ]. There exists a time regime, the late stage, where the time-dependent structure factor $S(Q,t)$ has scaling properties. They indicate the evolution of self-similar struc-

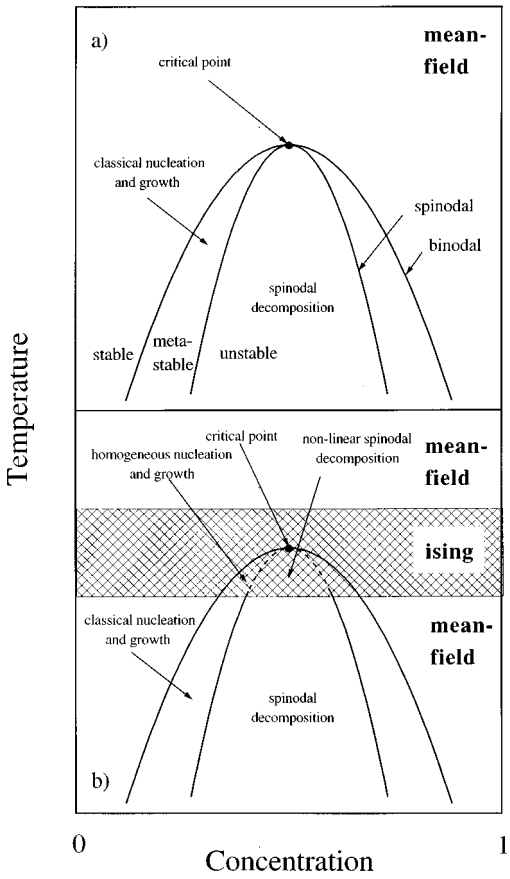

FIG. 1. Phase diagram for a binary mixture in mean-field approximation (a). The binodal separates the stable one-phase from the two-phase region, which is separated in the metastable and unstable regions by the spinodal. Two different phase separation processes occur in the two-phase region, the classical nucleation and growth in the metastable regime and the spinodal decomposition in the unstable regime. The phase diagram becomes more complex if one takes the 3D Ising regime into consideration (b). In the shaded two-phase region the phase separation is described as a transition from homogeneous nucleation and growth to nonlinear spinodal decomposition by strong fluctuations [22]. In this regime, the spinodal loses its physical significance though it can be formally found by extrapolation from the one-phase region.

tures. In particular, $S(Q,t)$ scales with a characteristic length $Q_m^{-1}(t)$, the inverse of the maximum position. It leads to the dynamical scaling hypothesis [16]

$$S(Q,t)=Q_m(t)^{-d}F(x), \tag{1}$$

with a time-independent normalized structure factor $F(x)$, with $x=Q/Q_m(t)$, and the Euclidean dimension $d=3$. This behavior was confirmed in many experimental studies, and we refer to the detailed monographs of Hashimoto [3] and Binder [4]. However, this exponent was controversially discussed for the blend of polystyrene and polyphenylmethylsiloxane (PS/PPMS). Nojima *et al.* obtained $d_f=2.38\pm0.48$ for various off-critical quenches and $d_f=2.77\pm0.3$ for critical quenches [17]. In contrast to these results, Takahashi *et al.* [18] as well as Kuwahara *et al.* [19] reported $d=3$, as expected.

Beyond this scaling, for $x>2$ the introduction of a second characteristic length was necessary. It was identified as the ''interface'' thickness of the domains l_I [20], which should be proportional to the critical correlation length [21]. However, in most experiments the second length was much larger than predicted [3,20].

In our experimental work we studied the blend of deuteropolystyrene and polyphenylmethylsiloxane (d-PS/PPMS) both with a molecular volume of $V=4300\ \mathrm{cm}^3/\mathrm{mol}$. We used small-angle neutron scattering (SANS) and photon correlation spectroscopy (PCS) for the investigation of the equilibrium properties. The nonequilibrium properties were studied by quenches from the one- into the two-phase region with time-resolved small-angle light scattering (SALS). We will mainly deal with three questions: (i) the influence of thermal concentration fluctuations on demixing after the quenches; (ii) the phase separation during its later stages, in order to investigate the scaling behavior and, in particular, the determination of the dimensionality d from Eq. (1) and deviations from $d=3$; and (iii) the ''second'' length scale and its relation to the interface thickness.

Our quenches end in the metastable regime as shown by combining different scattering techniques. By the determination of the Ginzburg number Gi we will show that strong concentration fluctuations exist in a wide temperature range. This will be discussed in the context of homogeneous nucleation, which occurs in the shaded region of Fig. 1(b), as proposed by Binder [22]. According to the Ginzburg criterion the amplitude of the concentration fluctuations becomes comparable to the difference of the concentrations determined by the binodal. Thus, contrary to the classical case, nucleation is much easier, because many small droplets can grow simultaneously in the sample. In particular, the spinodal loses its physical significance, and, seemingly, homogeneous nucleation cannot be distinguished experimentally from spinodal decomposition. Consequently, we analyze our data with the scaling concepts of spinodal decomposition and use its terminology. But, in contrast to the mean-field case the ''early stage'' of spinodal decomposition does not appear at all in the Ising regime because of the large fluctuations.

II. THEORETICAL CONCEPTS

A. Equilibrium properties and static structure factor

In the mean-field regime of the one-phase region, the static structure factor $S(Q)$ of binary polymer blends is described by the random phase approximation (RPA) [1] to be

$$S^{-1}(Q)=S_1^{-1}(Q)+S_2^{-1}(Q)-2\Gamma \tag{2}$$

with the structure factors S_i, $i=1,2$, for the polymer species 1 and 2,

$$S_i(Q)=2\Phi V_i\{y-1+\exp(-y)\}/y^2. \tag{3}$$

The generalized Flory-Huggins interaction parameter Γ is a free energy in units of RT (R gas constant), namely, $\Gamma=\Gamma_h/T-\Gamma_\sigma$, with Γ_h and Γ_σ the enthalpic and entropic term, respectively [4]. It is a segmental quantity; i.e., it does not depend on the degree of polymerization N. Φ is the concentration, V_i is the molecular volume of one of the chain

components, and $y=Q^2R_g^2$ is related to the momentum transfer Q and the radius of gyration R_g. Equation (3) is the Debye function for a Gaussian coil. For the limiting case $QR_g \leqslant 1$ one obtains the Zimm approximation

$$S^{-1}(Q)=S^{-1}(0)+AQ^2 \tag{4}$$

with the inverse forward scattering

$$S^{-1}(0)=\left\{\frac{1}{\Phi V_1}+\frac{1}{(1-\Phi)V_2}\right\}-2\Gamma=2(\Gamma_S-\Gamma). \tag{5}$$

The slope A depends on the conformations

$$A=\frac{1}{3}\left\{\frac{R_{g,1}^2}{\Phi V_1}+\frac{R_{g,2}^2}{(1-\Phi)V_2}\right\}. \tag{6}$$

Γ_S is the Flory-Huggins parameter at the spinodal temperature. It is determined by the molecular volumes and the concentration. For similar chains with $R_{g,1}\approx R_{g,2}$ and $V_1\approx V_2$ this yields

$$S^{-1}(0)=[\Phi(1-\Phi)\overline{V}]^{-1}-2\Gamma \quad \text{and}$$

$$A=\overline{R_g^2}/[3\Phi(1-\Phi)\overline{V}]. \tag{7}$$

$\overline{R_g}$ is the mean value of the radius of gyration and $\overline{V}$ the mean molecular volume. The inverse forward scattering is a susceptibility, connected to thermodynamics by the relation

$$S^{-1}(0)=\partial^2(\Delta G/RT)/\partial\Phi^2. \tag{8}$$

The inverse of Eq. (4) is the Ornstein-Zernike formula

$$S(Q)=S(0)/(1+\xi^2Q^2) \tag{9}$$

with the correlation length $\xi=\sqrt{AS(0)}$. In the asymptotic regimes near and far from the critical point, the temperature dependence of forward scattering and correlation length are given by simple scaling laws

$$S(0)=C\epsilon^{-\gamma}, \quad \xi=\xi_0\epsilon^{-\nu}, \tag{10}$$

respectively, with the reduced temperature $\epsilon=|T-T_c|/T$ and the critical temperature T_c. Far from the critical point the extrapolated mean-field critical temperature is T_c^{MF}, the critical amplitudes are C_{MF} and ξ_{MF}, and the critical exponents are $\gamma=1$ and $\nu=0.5$. In the region close to the critical point the fluctuations grow and are mutually correlated. In the universality class of the three-dimensional (3D) Ising model one gets the critical temperature T_c, the critical exponents $\gamma\cong 1.24$, $\nu\cong 0.63$, and the critical amplitudes C_+,ξ_+. Whereas the scaling laws in Eq. (10) are only valid in the asymptotic regions, the following general crossover function [8] holds:

$$\hat{\epsilon}=(1+2.333\hat{S}(0)^{\Delta/\gamma})^{(\gamma-1)/\Delta} \times\{\hat{S}^{-1}(0)+[1+2.333\hat{S}(0)^{\Delta/\gamma}]^{-\gamma/\Delta}\}. \tag{11}$$

It approximates the susceptibility over the whole one-phase regime including the asymptotic mean-field and 3D Ising regimes. Equation (11) is a universal function with the scaled quantities $\hat{\epsilon}=\epsilon/\mathrm{Gi}$ and $\hat{S}(0)=\mathrm{Gi}S(0)/C_{\mathrm{MF}}$ where Gi is the Ginzburg parameter. It is developed from an ϵ expansion based on renormalization-group analysis, and yields Gi and C_{MF} as fit parameters. The Ginzburg number Gi is defined as the reduced temperature $\epsilon^*\equiv(T^*-T_c)/T^*$ at which the deviation of the data from the Ising model [Eq. (10)] approaches 10%. $C_{\mathrm{MF}}=1/[2(\Gamma_c+\Gamma_\sigma)]$ is expressed by the entropic part of the Flory-Huggins parameter Γ_σ and its value at the critical point Γ_c, which is related to the entropy of mixing and proportional to $1/N$ [Eq. (5)].

B. Dynamical structure factor

The relaxation of concentration fluctuations in the one-phase region close to the equilibrium value Φ is described by the dynamical structure factor [23,24]

$$S_d(Q,t)=S(Q)\exp(-t/\tau). \tag{12}$$

The relaxation time τ is related to the interdiffusion coefficient D_c according to

$$\tau^{-1}=D_cQ^2. \tag{13}$$

Equation (13) is valid in the hydrodynamic regime $Q\xi\ll 1$. Close to the critical point we can reach $Q\xi>1$ and a regime exists where mode coupling corrections have to be considered. In particular, a transition from Q^2 to Q^3 behavior is theoretically predicted and confirmed experimentally [25]. Neglecting mode coupling effects in the 3D Ising regime the temperature dependence of the diffusion coefficient reads

$$D_c=\epsilon^\gamma D_0\exp(-E_A/RT), \tag{14}$$

with $\gamma\cong 1.24$. The Arrhenius form for the kinetic factor is multiplied with the ϵ^γ term which follows the usual critical slowing down of the interdiffusion process in the vicinity of the critical temperature T_c. E_A is the activation energy assuming the diffusion is caused by a thermally activated process. The slowing down near the glass transition temperature T_G was neglected because our blend was always far from T_G.

C. Phase decomposition

After a temperature quench from the thermodynamically stable one-phase into the unstable two-phase and mean-field region, the system decomposes. The corresponding equilibrium concentrations are determined by the binodal. If the sample is quenched into the metastable regime, phase separation occurs by nucleation and growth; e.g., the thermal concentration fluctuations of the concentration have to overcome a barrier before becoming unstable and driving the phase separation. On the other hand, if the sample is quenched into the unstable regime the phase decomposition occurs by the growth of the unstable long-wavelength modes. This is the process of spinodal decomposition. Its time evolution can be tentatively classified into three regimes [3]. In the early stage the concentration fluctuations are small and uncorrelated. They are described analytically by the linear Cahn-Hilliard-Cook theory. There is a maximum growth rate of concentration fluctuations at a constant wave number $Q_m=2\pi/\Lambda_m$. For small times the unstable fluctuation

modes grow exponentially with time. In the intermediate and late stages the concentration fluctuations interact with each other and are described by a nonlinear equation where no analytic expression exists. In a more sophisticated picture [26] a fourth time regime was proposed, namely, the transition stage between intermediate and late stages, called the final stage in that paper.

D. Scaling concepts in phase separation

In scattering experiments the domain structure and its time evolution are measured by the time-resolved static structure factor $S(Q,t)$. The domain structure in the late stage of spinodal decomposition is supposed to be characterized as an evolution of a self-similar structure. Therefore, it is possible to describe the decomposition process by a scaling function that only depends on a single characteristic length, which depends on time. It should become independent of system properties such as the molecular volume V and the quench depth ΔT. Thus $S(Q,t)$ should follow a master curve if scaled with the characteristic length of the decomposition process. This length is identified with the inverse wave number of the intensity maximum $Q_m(t)^{-1}$ leading to Eq. (1). The time-independent structure factor $F(x)$ is proportional to the mean square deviation of the concentration from its mean value Φ:

$$F(x) \propto \langle \delta\Phi^2 \rangle. \tag{15}$$

$F(x)$ grows during the early and intermediate stages of phase separation. In the intermediate stage the mean concentrations of the developing domains change until they reach their equilibrium values Φ' and Φ'' on the binodal, and we introduce $\Delta\Phi = \Phi' - \Phi''$ (Fig. 1). From then on $F(x)$ stays constant during the late stage. Thus a time-independent scaling function $F(x)$ indicates the beginning of the late stage.

Another criterion to identify this time regime is the integrated square of the order parameter. It is proportional to the second moment of the scattered intensity

$$\int_0^{Q^*} \langle \delta\Phi^2(t) \rangle Q^2 dQ \propto \int_0^{Q^*} S(Q,t) Q^2 dQ \tag{16}$$

with an upper integration limit Q^* determined by the experiment. Plotting the second moment versus time [Eq. (16)] the beginning of the late stage is characterized by the inset of a plateau. This also indicates that the thermal concentration fluctuations of concentration on length scales equal to or smaller than $1/Q^*$ reach equilibrium. On the other hand integration of Eq. (16) to $Q \to \infty$ would include scattering from concentration fluctuations for all length scales, and therefore the second moment would be constant for all times and proportional to $\Phi(1-\Phi)$.

The scaling function normalized for different quench temperatures T_f according to $\overline{F} \propto F / \int_0^{Q^*} \langle \delta\Phi^2 \rangle dQ$ can be approximated by [27]

$$\overline{F(x)} = x^n (1 + \eta/n) / (\eta/n + x^{n+\eta}) \tag{17}$$

with $2 \leqslant n \leqslant 4$, $\eta = d+1$ for $\Phi < 0.16$ and $\eta = 2d$ for $\Phi \geq 0.16$. So far, no conclusive and general derivation for $F(x)$ exists. For small x theoretical predictions exist with $n = 2$ [27] as well as $n = 4$ [28,29]. $\overline{F(x)}$ in Eq. (17) is normalized to $F(1) = 1$. The concentration $\Phi = 0.16$ is the limit of percolation [27]. This scaling function is applied to interpret our data.

E. Scaling of Q_m and S_m

During the time evolution of the spinodal decomposition in the intermediate and late stages, the position of the scattering maximum Q_m shifts to smaller values, and the peak intensity $S_m(t) \equiv S(Q_m(t),t)$ increases. The decrease of Q_m is related to coarsening, whereas the increase of S_m is related to the increase of $\delta\Phi$ and to the coarsening of the domains as well. The time evolution of $Q_m(t)$ and $S_m(t)$ is approximately described by power laws according to

$$Q_m(t) \propto t^{-\alpha(t)} \quad \text{and} \quad S_m(t) \propto t^{\beta(t)}. \tag{18}$$

The exponents α and β depend on the different coarsening mechanisms during decomposition. Therefore they can change with time in going from one regime to another. Eliminating t one gets from Eq. (18)

$$S_m \propto Q_m^{\sim(\beta/\alpha)} \tag{19}$$

For the late stage this leads to the relationship $\beta/\alpha = d$ from Eq. (1), i.e., $d = 3$ in the case of compact structures. During the intermediate stage the exponents α and β lead to $\beta/\alpha > d$. The underlying reason is the time-dependent growth of the difference of concentration $\delta\Phi$ in both phases.

For the quantities $Q_m(t)$ and $S_m(t)$ one also obtains a master curve with the same arguments as for $S(Q,t)$, provided that these quantities and the time are scaled with the collective diffusion coefficient and the correlation length. This leads to [30]

$$\overline{Q_m}(\overline{t}) = \sqrt{2} Q_m(t) \xi(T), \quad \overline{S_m}(\overline{t}) = 2\sqrt{2} \xi^3(T) S_m(t),$$
$$\overline{t} = t \cdot D_c / (2\xi^2) \tag{20}$$

and yields the dimensionless quantities $\overline{Q_m}(\overline{t})$, $\overline{S_m}(\overline{t})$, and the reduced time $\overline{t}$. The plots of $\overline{Q_m}(\overline{t})$ and $\overline{S_m}(\overline{t})$ are supposed to follow a master curve independent of the polymer properties and temperature T_f.

F. Other characteristic length scales: ''Local properties'' of the domain interface

The basic assumption of scaling during the late stage of spinodal decomposition is that the precipitated domain structure is self-similar and characterized by a single length scale. There are, however, other characteristic lengths in the system that determine what we call ''local'' properties. These are essentially the thickness or an eventual waviness of the domain interface. There are other scales as the correlation length of thermal concentration fluctuations and the dimension of the coil, i.e., its radius of gyration and statistical segment length, which are beyond the accessible Q range of our spectrometer, and which are not considered for the moment. Scaling by a single length is observed if the domain size is of the order of μm and much larger than the other lengths which are typically of the order of 100 Å.

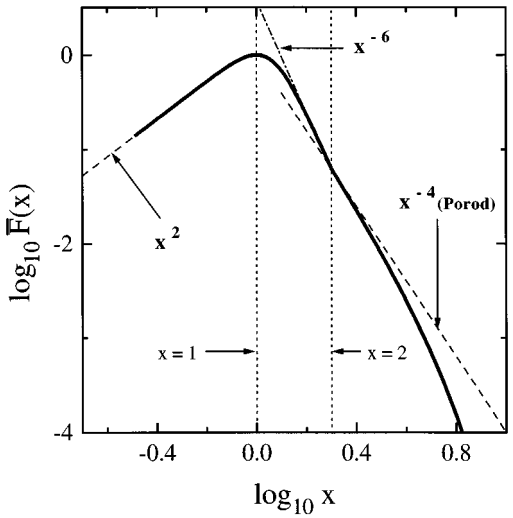

FIG. 2. Schematic picture of the scaled structure factor $\overline{F(x)}$ versus the scaled scattering vector $x=Q/Q_m$ in the late stage of spinodal decomposition. The curvature of the function for $x>2$ deviating from Porod's law is caused by the domain interface, with a second characteristic length.

Therefore, in order to reveal these local properties experiments have to be performed at larger Q values. For $Q>2Q_m$ (i.e., $x>2$) one expects the validity of Porod's law [20]

$$S(Q,t)=P(t)Q^{-4}\exp[-l_I(t)^2Q^2/2\pi] \tag{21}$$

with the interface thickness l_I and Porod's constant P, which is proportional to the surface of the domains per volume element. Equation (21) leads to Porod's scattering law for a negligible interface thickness ($l_IQ\ll 1$). In equilibrium and in the mean-field approximation the interface thickness is related to the correlation length of the thermal concentration fluctuations [21]

$$l_I=2\sqrt{2}\,\xi(T). \tag{22}$$

From Eq. (21) one obtains the scaling function for $x>2$, namely,

$$F(x)=\hat{P}x^{-4}\exp(-\hat{l}_I^2x^2/2\pi) \tag{23}$$

with the normalized Porod constant $\hat{P}=Q_m(t)^{(d-4)}P(t)$ and the normalized interface thickness $\hat{l}_I=l_I(t)Q_m(t)$. Thus, combining the scaling functions of Eq. (17) ($x<2$) together with Eq. (23) ($x>2$) one gets a scaling function for $S(Q,t)$ for a larger Q or x range, describing the time evolution of the domains including the properties at their interface. This scaling function is depicted in Fig. 2. If $F(x)$ follows a master curve also for $x>2$, the second length of the domain structure is negligibly small or it follows the time law of the domain size itself. Finally, it has to be mentioned that the above discussed formalism of scaling does not include scattering from the thermal concentration fluctuations inside the domains because they are not visible in our Q range.

TABLE I. Characteristic properties of the components d-PS and PPMS.

	d-PS	PPMS
ρ (g/cm^3)	1.130	1.143
m (g/mol)	112	136
Ω (cm^3/mol)	99.1	119
M_W (g/mol)	4900	4900
V_W (cm^3/mol)	4340	4290
u	1.04	1.08
N	44	36
T_G (°C)	76	−26

III. EXPERIMENTAL SECTION

A. Sample preparations

The blend of deuterated polystyrene (d-PS) and polyphenylmethylether (PPMS) shows an upper critical solution temperature (UCST), which means that it is homogeneously mixed at high temperatures and phase separated at low temperatures. The d-PS polymer was purchased from Polymer Science Standards (PSS) in Mainz and the PPMS polymerized at the Max-Planck-Institute for Polymer Research in Mainz. Both were synthesized by anionic polymerization. The molecular weight was determined by gel permeation chromatography with a value of $M_W=4900$ g/mol and a polydispersity better than $u=1.1$ defined as the ratio of the weight and number averaged molecular weights M_W and M_n, respectively. The characteristic parameters are summarized in Table I. A sample of nearly critical composition, namely $\Phi_{d\text{-PS}}=0.51$, was mixed for 30 min at a temperature between 100 °C and 120 °C. A homogeneously mixed sample was obtained, as confirmed by SANS experiments. The preparation was carried out under air because the relatively short chains of our sample do not react with oxygen and water up to 170 °C. For the SANS experiments sample material of 1-mm thickness was filled into a containment, which had a 1-mm niobium back window and a front window of 2-mm boron-free quartz glass. For the SALS experiments optical pure quartz glass (suprasil) was used from Hellma in Mühlheim/Baden. The cell had a 22-mm inner diameter and 1-mm thick front and back windows. The samples were 0.1 and 0.01 mm thick. For the PCS experiments, another procedure was required to sufficiently reduce parasitic light scattering from impurities. After dissolving the polymer mixture in benzene it was purified by filtering several times. Then the solution was filled into a 10-mm-thick cylindrical cell and freeze dried. Afterwards the cell was filled with argon and molten off.

B. Small-angle neutron scattering

The SANS experiments were performed with the small-angle neutron diffractometer at the Risø National Laboratory in Denmark. The entrance slit was a square of 1 cm^2. The neutron wavelength of 7 Å was selected with a mechanical selector having a resolution of $\Delta\lambda/\lambda=0.18$. The distance between sample and area sensitive detector was 6 m. The resulting range of scattering vectors was 10^{-2} Å$^{-1}<Q$

$<4\times10^{-2}$ Å^{-1} with $Q=4\pi\sin(\theta/2)/\lambda$. The temperature control system provided a stability better than 0.1 K.

The scattering curves were corrected for background and inhomogeneous detector efficiency. Corrections for incoherent and multiple scattering were not necessary. The data were calibrated in absolute units with a vanadium-calibrated Lupolen standard. The structure factor $S(Q)$ was then calculated from the macroscopic cross section $d\Sigma/d\Omega$ with the relation

$$S(Q)=\frac{d\Sigma}{d\Omega}(Q)(N_A/\Delta\rho^2). \tag{24}$$

$\Delta\rho$ is the difference of the coherent scattering length densities between the blend components, and N_A is the Avogadro number.

C. Photon correlation spectroscopy

The PCS experiments were performed at the Max-Planck-Institute for Polymer Research in Mainz. The intensity–time-correlation function $G(Q,t)$ was measured at a fixed angle of $\theta=90°$. The light source was a Neodym-YAG laser operating at $\lambda=533$ nm, which yields $Q=2.6\times10^{-3}$ Å^{-1} at $\theta=90°$ with $Q=4\pi n\sin(\theta/2)/\lambda$ (n is the refractive index of the medium). A temperature stability better than 0.5 K was achieved by a metal heater. The normalized dynamical structure factor $g(Q,t)=S_d(Q,t)/S(Q)$ [31] is evaluated from $G(Q,t)$ if measured under homodyne conditions by

$$G(Q,t)=\langle I(Q)\rangle^2(1+fa^2|g(Q,t)|^2). \tag{25}$$

$S_d(Q,t)$ and $S(Q)$ are the respective dynamical and static structure factors already introduced, and $\langle I(Q)\rangle$ is the time average of the scattered light intensity. The number f is an instrumental factor, a is known from the fraction of the total scattered intensity $I(Q)$ which belongs to a selected relaxation process. Corrections for multiple scattering were not necessary under the present experimental conditions.

D. Small-angle light scattering

The time-resolved light scattering experiments were also performed at the Max-Planck-Institute for Polymer Research in Mainz. The light of a He-Ne laser with $\lambda=633$ nm (Q range 10^{-4} Å$^{-1}<Q<7\times10^{-4}$ Å^{-1}) passes a metal heater (temperature stability better than 0.05 K) and then hits the sample. The scattered light falls onto a scattering screen made of frosted glass and, after reemission, was recorded by the position-sensitive CCD (charge coupled device) detector of a video camera. The primary beam passes the screen through a hole and is reflected into a photodiode to determine instantaneously the transmission. Intensities varying up to four decades could be detected by using different diaphragm diameters.

We have to apply several corrections for the data reduction: first, after radial averaging the detected intensity was corrected for the deadtime of the CCD detector, which led to a correction factor depending linearly on the counted intensity [32] and gave a 40% correction for the highest intensity. Secondly, the parasitic scattering times the transmission coefficient was subtracted from the scattered intensity. The transmission was found between 0.85 and 1. Parasitic scattering came from the heating windows, the sample cell, and dust and was measured at high temperatures with the sample in its mixed state. The scattering from thermal concentration fluctuations was negligible. Thirdly, the resulting raw data were corrected for effects due to the scattering geometry [33], e.g., the distance r between the flat screen and the sample depends on the scattering angle θ, which results in a correction for the r^{-2} decrease of the scattered intensity. Fourthly, the reemitted intensity was corrected for the anisotropic reemission probabilities of the screen, which depend on the angles of incidence and emission. This correction factor was determined by a calibration of the screen using an aqueous solution of latex spheres [32]. For a sphere radius of $R_s\cong2000$ Å and a volume fraction of $\Phi=6.2\times10^{-5}$ the scattering law $S(Q)$ is theoretically described by the form factor of spheres. In Fig. 3 the measured intensity of the aqueous solution (circles) is compared with the theoretical form factor (dashed line). Interparticle effects were shown to be negligible. The full line is a fit with the form factor using a larger radius $R_s\cong2400$ Å. Dividing both theoretical curves we achieved the correction factor for the anisotropic reemission, which is plotted as the inset in Fig. 3. It amounts up to 30% for large Q values. We should remark that the calibration could also be used to get the scattered intensity in absolute units, i.e., the calibrated cross section $d\Sigma/d\Omega$ in units (1/cm) [32]. Finally, the data were multiplied with empirical conversion factors accounting for different diaphragm diameters. To demonstrate the influence of all applied corrections one data set before and after correction is plotted in Fig. 4. It can be seen that the corrections lead to smaller intensity values for low Q values mainly because of the background subtraction whereas one gets larger values at higher Q's due to the geometrical and screen corrections. These corrections are very important. Even the value of Q_m is shifted by them.

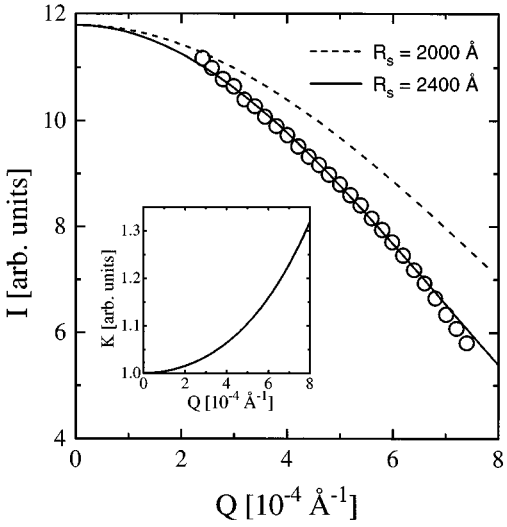

FIG. 3. Characteristic reemission-efficiency of the SALS spectrometer screen. The intensity I of an aqueous solution of latex spheres with a concentration $\phi=6.2\times10^{-5}$ is plotted vs the scattering vector Q (circles). The fitted form factor of the spheres with $R_s=2400$ Å (full line) is compared with the calculation for the actual radius $R_s=2000$ Å (dashed line). The ratio of both leads to a correction factor for the efficiency (inset).

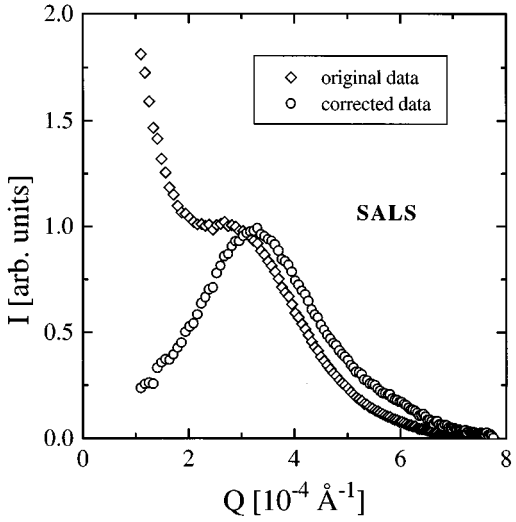

FIG. 4. Intensity I of an arbitrary data set measured with SALS vs scattering vector Q before (diamonds) and after (circles) data reduction includes also the correction for parasitic scattering at small Q values. For larger Q the scattering geometry and the screen efficiency are dominating according to the results in Fig. 3.

IV. RESULTS AND DISCUSSIONS

A. Equilibrium structure factor, phase boundaries, and Ginzburg number from SANS

Figure 5(a) shows the equilibrium structure factor $S(Q)$ in a Zimm representation for different temperatures $T>T_B$ in the one-phase region measured with SANS. The data follow the theoretical least-square fit of Eq. (4) for all temperatures. Figure 5(b) is a plot of the structure factor for temperatures $T<T_B$ in the two-phase region after phase separation. At large Q the scattering data follow a straight line as in the one-phase region. They represent the equilibrium thermal concentration fluctuations in the domains. Their intensity decreases for lower temperatures because the distance from T_c increases. At small Q a deviation from the theoretical straight lines is observed, which increases for lower temperatures. The very high intensity in this Q range results from the scattering by the phase-separated domains. This indicates that the quench temperature reaches the two-phase region of the phase diagram. Thus one can distinguish between the one- and the two-phase region with SANS, and we obtain directly the binodal temperature at $T_B=(123.5\pm0.5)$ °C.

In Fig. 6 the temperature dependence of the inverse forward scattering $S^{-1}(0)$ is plotted in scaled quantities [Eq. (11)] for $T>T_B$. The full line represents the least-square fit of the crossover function [Eq. (11)] yielding the spinodal temperature $T_S=(119.5\pm0.1)$ °C. Thus, the SANS experiments show that the blend is slightly *off* the critical concentration. The width of the metastable region, i.e., the gap between binodal and spinodal is determined to be $\Delta T_M\equiv(T_B-T_S)\cong4$ K.

Obviously, the quenches penetrate deeply into the Ising regime; even for temperatures $\Delta T\equiv(T-T_S)\cong50$ K we still find $\hat{\epsilon}=\epsilon/\mathrm{Gi}<1$. The Ginzburg number $\mathrm{Gi}=0.48\pm0.14$ obtained from the fit in Fig. 6 is much larger than for simple liquids ($\mathrm{Gi}\cong10^{-2}$). This underlines that our system follows the 3D Ising model over a wide temperature range, leading to strong thermal concentration fluctuations. Previous SANS results on the same system [34] confirmed that even in the phase-separated domains, the equilibrium fluctuations are still *comparable to the order parameter itself.*

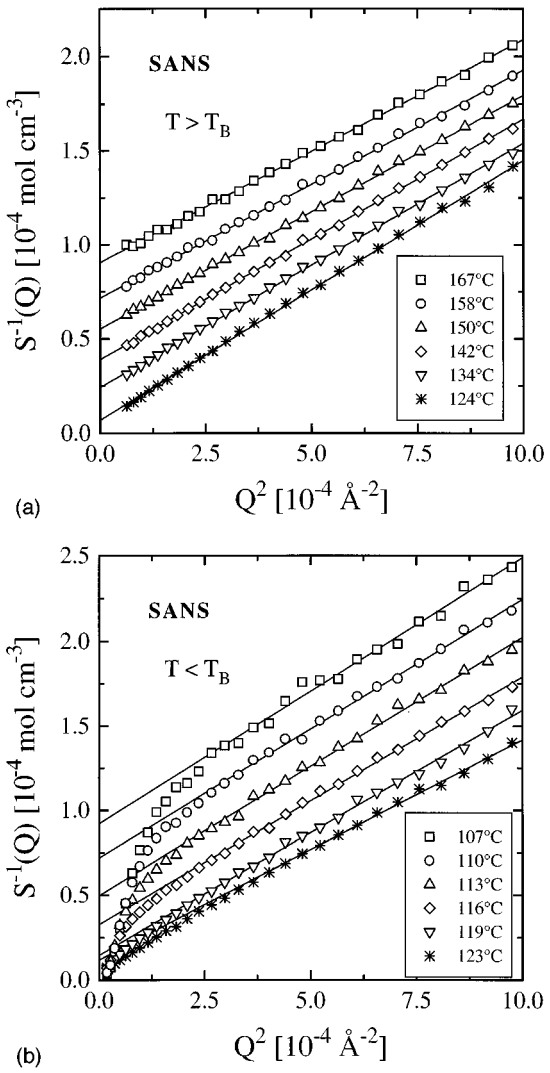

FIG. 5. (a) The structure factor $S(Q)$ measured with SANS and plotted in a Zimm representation for various temperatures $T>T_B$ in the one-phase region. The full lines are least-square fits with Eq. (4). (b) Various data sets in the same representation for $T<T_B$ in the metastable regime. The full lines fitted with Eq. (4) describe the thermal concentration fluctuations inside the phase separated domains. Additional scattering of the precipitated domains leads to deviations from the solid lines for small Q values. The statistical error bars are always less than the size of the symbols.

The correlation length ξ evaluated from Eq. (9) is plotted in Fig. 7 versus the reduced temperature in a double logarithmic scale. A linear regression fit gives $\xi_+=9.0\pm0.1$ Å and the critical exponent $\nu=0.633\pm0.003$, as predicted by the 3D Ising model in Eq. (10).

B. Diffusion coefficient and an ''extra'' slow relaxation process

Photon correlation spectroscopy was used to determine the collective diffusion coefficient D_c of the mixture for various temperatures $T>T_B$. In Fig. 8 four exemplary spectra of

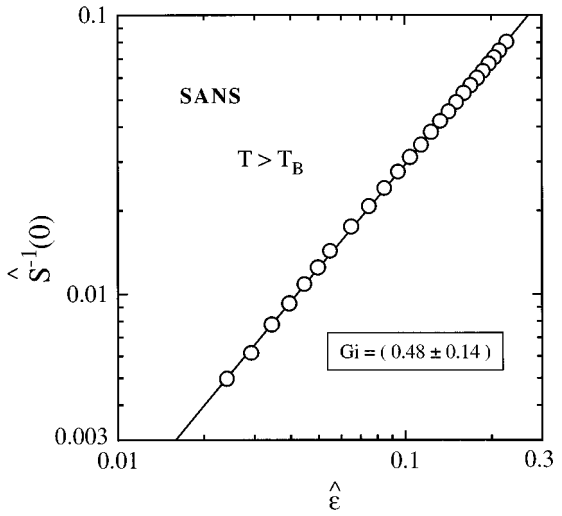

FIG. 6. Rescaled inverse forward scattering $\hat{S}^{-1}(0)$ vs rescaled reduced temperature $\hat{\epsilon}$ in a double logarithmic scale. The full line is a fit with the crossover function of Belyakov and Kiselev [8]. All data are taken deep in the Ising regime ($\hat{\epsilon}<1$). The resulting Ginzburg number $\mathrm{Gi}=0.48\pm0.14$ is much larger than for simple liquids.

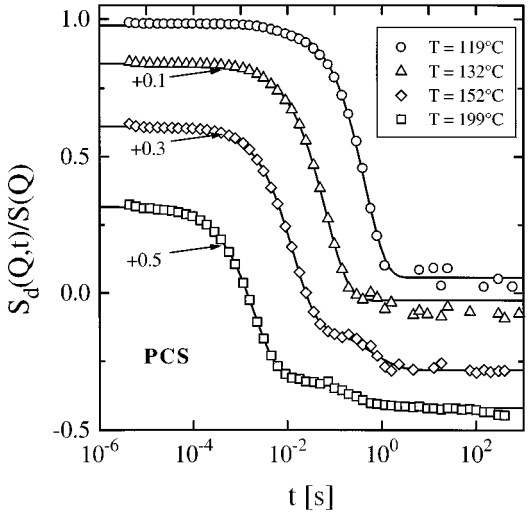

FIG. 8. Normalized dynamic structure factor $S_d(Q,t)/S(Q)$ vs time t in a semilogarithmic plot for different temperatures T in the one-phase region measured with PCS. The step is caused by the concentration fluctuations. A second and very slow relaxation process appears for higher temperatures. The full lines are least-square fits with Eq. (12) supplemented by an additional exponential for the slow relaxation process. Various shift factors are used for better representation.

the normalized dynamical structure factor $S_d(Q,t)/S(Q)$ are depicted versus time in a semilogarithmic scale. The steep decrease of the correlation function at $t\cong10^{-3}$ s is related to the relaxation process of the concentration fluctuations. Surprisingly, an additional very slow relaxation process is observed in a time region of about 0.1 s for temperatures 152 °C and 199 °C. This will be discussed at the end of this section. The full lines in Fig. 8 were obtained by fitting Eq. (12) and adding a second exponential.

The diffusion coefficient was then calculated according to Eq. (13) because mode coupling effects can be neglected. This was proven by determining the temperature where the relaxation times show a transition from the Q^2 dependence of Eq. (13) in the hydrodynamic regime ($Q\xi\ll1$), to a non-diffusive Q^3 behavior ($Q\xi>1$). To measure at different Q values or scattering angles we had to use another spectrometer, which, unfortunately, provided only temperatures up to 140 °C. Therefore, we prepared another mixture of the same blend with slightly smaller molecular weight in order to shift the spinodal to lower temperatures. The PCS experiments for this mixture were performed at scattering angles between $\Theta=30°$ and 150° in the one-phase region. Plotting the inverse relaxation time τ^{-1} versus Q in a double logarithmic scale we determined the exponent α^* according to $\tau^{-1}=DQ^{\alpha^*}$. A deviation from the Q^2 dependence was only detected for $\Delta T\equiv(T-T_S)\leqslant9$ K above the spinodal. Only in this temperature range mode coupling corrections had to be considered. Therefore, for temperatures $\Delta T\geqslant9$ K the diffusion coefficient could be reliably calculated from Eq. (13). The results for this mixture were also valid for the original blend because their critical amplitudes ξ_+ differ only by 0.1 Å, which was confirmed by SANS experiments. In Fig. 9 the collective diffusion coefficient, calculated from Eq. (13), is plotted in a semilogarithmic scale versus the inverse temperature. The full line is a least-square fit of Eq. (14) yielding an activation energy of $E_A=43\pm3$ kJ/mol. Approaching the spinodal, the deviation of D_C from the Arrhenius straight line (dashed) reveals the increasing influence of the thermodynamic factor in Eq. (14) leading to the well-known critical slowing down. An additional slowing down that might appear approaching the glass transition temperature T_G was not observed. (T_G of the blend was between 120 and 200 K below the experimental temperatures.) Previous SANS experiments confirmed that an Arrhenius behavior of the diffusion was still valid even 50 K above the glass transition for an isotopic mixture of polystyrene [35].

Finally, we discuss the unexpected additional relaxation process. In blends, slow processes with relaxation times of

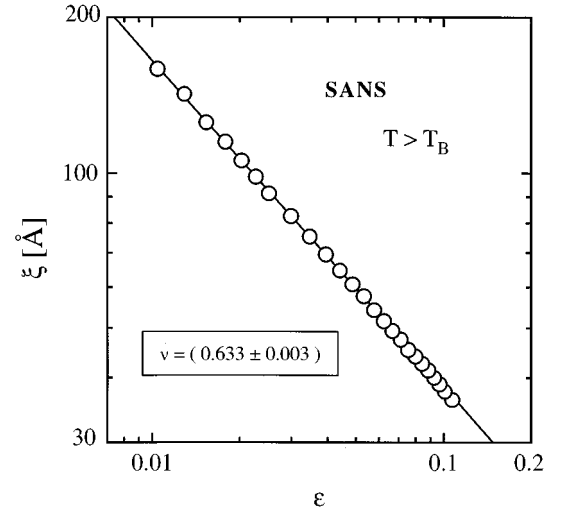

FIG. 7. Double logarithmic plot of the correlation length ξ vs the reduced temperature ϵ in the homogeneous region $T>T_B$. Fitting the data with Eq. (10) gives the correct critical exponent $\nu=0.633\pm0.003$ for the 3D Ising model.

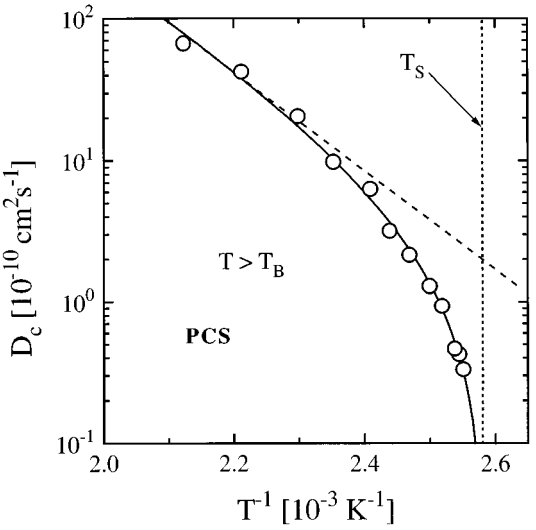

FIG. 9. Collective diffusion coefficient D_c vs inverse temperature T^{-1} for $T>T_B$. The full line is a fit with Eq. (14). The critical slowing down appears as a curvature deviating from the dashed Arrhenius line. The extrapolation to the spinodal temperature T_S is shown by the dotted line.

seconds were already observed by several groups. It seems that these slow processes are generally related to density fluctuations. In glass-forming liquids a slow relaxation process was observed near the glass transition T_G and related to so-called density ''clusters'' [36]. However, the glass transition temperature for our mixture is about 200 K below the experimental temperature, as discussed in the last section. So we conclude that the observed slow processes in Fig. 8 have nothing to do with the glass transition. Two publications report such a slow process in binary polymer mixtures: in an asymmetric critical mixture of low molecular polystyrene and polybutadien Hair *et al.* [37] discovered such a process at different scattering angles and temperatures with time scales as observed by us. These authors relate the slow process to the ''Fisher renormalized'' critical behavior, which occurs if a third component is present in the system and starts to fluctuate. It is plausible to relate the observed slow process to such density fluctuations, associated with the free volume or loose packing of the blend. A slow process was also observed by Meier *et al.* [38] in the same blend as used in our work, but with slightly different molecular weight and at temperatures closer to the glass transition temperature. All evaluated equilibrium properties of the mixture are summarized in Table II.

TABLE II. Experimental equilibrium results of the *d*-PS/PPMS blend determined by SANS and PCS.

T_B (°C)	123.5±0.5
T_S (°C)	119.5±0.1
ΔT_M (K)	4
Gi	0.48±0.14
ξ_+	9.0±0.1
ν	0.633±0.003
E_A (kJ/mol)	43±3

C. Late stage of spinodal decomposition

The experiments to investigate the decomposition processes were performed with time-resolved small-angle light scattering. Before starting the actual quench experiments we determined the boundary between the one- and two-phase region by neutron scattering experiments (see Sec. IV A). Phase separation first appeared at the cloud-point temperature $T_{cl}=116.8$ °C whereas the blend was still homogeneously mixed at a temperature 0.1 K above T_{cl}. The scattered intensity did not change even after 4 h. Previous experiments on the same blend with slightly different molecular weight confirmed that the cloud-point temperature T_{cl}, as determined by light-transmission measurements, can be identified with the binodal temperature T_B, as determined by SANS. Both methods were applied on the same sample in the same sample cell and under the same experimental conditions allowing direct comparison [39]. We were sure that our quenches started above the binodal temperature T_B. Small differences of the absolute values of our binodal temperatures measured by SANS and SALS are due to the different experimental setups [40].

The samples were rapidly cooled from an equilibrium state in the one-phase region down to a ''final'' temperature T_f within the two-phase region with quench depths $\Delta T_B \equiv T_B - T_f$ between 0.2 and 2.6 K. From the SANS experiments (see Sec. IV A) we know that the gap between binodal and spinodal is $(T_B - T_S) \cong 4$ K. So we conclude that all quenches ended in the metastable regime. Furthermore, from the large Ginzburg number we learn that the thermal concentration fluctuations are very strong: their amplitude $\delta\Phi$ is expected to approach the difference of the coexistence concentrations, i.e., $\Delta\Phi \cong \Phi' - \Phi''$. In this region [shaded in Fig. 1(b)], the fluctuations are strong enough to overcome the barrier of the classical heterogeneous nucleation. This leads to spontaneous formation of many droplets everywhere in the system, and, consequently, to homogeneous nucleation and growth, as predicted by Binder [22]. So, due to the strong thermal concentration fluctuations, the spinodal as extrapolated from $S^{-1}(Q=0)$ looses its physical meaning for the nonequilibrium properties in the region close to the top of the miscibility gap. However, we still apply the terminology and theoretical concepts developed for the late stages of spinodal decomposition.

Figures 10 and 11 show the scattered intensity $I(Q,t)$ versus the scattering vector Q for the shallowest and the deepest quenches. In both figures a scattering maximum appears that shifts to smaller Q values with increasing time. For the deeper quench the experimental Q window was passed 20 times faster and with a five times higher intensity. The position $Q_m(t)$ of the scattering maximum and the maximum intensity $I_m(t)$ are plotted versus time in Figs. 12 and 13 in a double logarithmic scale.

The transition from the intermediate to the late stage is sketched by the dashed line. The exact transition times t_l were obtained from the time evolution of the mean square deviation of the concentrations, evaluated from the second moment of the scattered intensity [Eq. (16)]. Typical data are plotted in Fig. 14 for $\Delta T_B = 0.4$ K. A plateau clearly appears after a time t_l when the concentrations have reached their equilibrium value determined by the binodal. This indicates

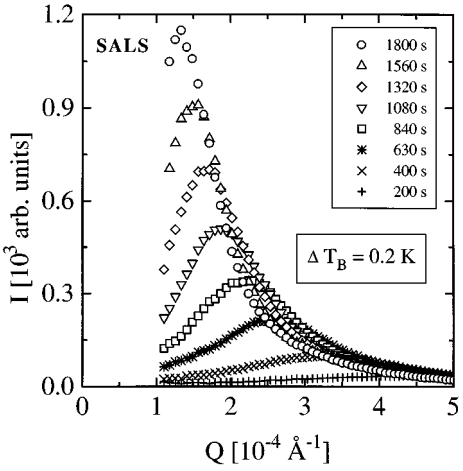

FIG. 10. Intensity I vs Q for the shallowest quench $\Delta T_B = 0.2$ K measured with SALS. The maximum grows and shifts to smaller Q values with increasing time.

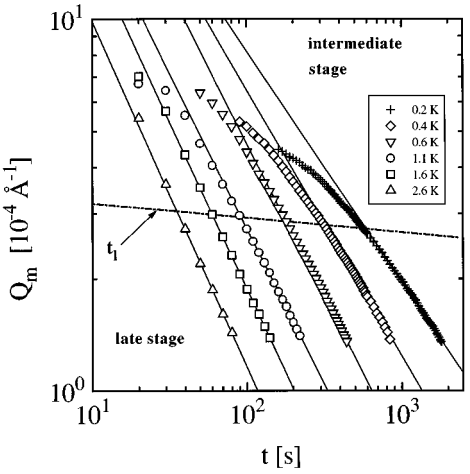

FIG. 12. Double logarithmic plot of the position Q_m of the scattering maximum versus time for different quench temperatures. The dashed line indicates the times t_l for the transition from the intermediate to the late stage. Q_m follows a simple power law in the late stage whose exponents are obtained from the straight lines.

the beginning of the late stage of decomposition. The exponents α and β in Eq. (18) were obtained from the slope of the fitted straight lines in Figs. 12 and 13. Only a weak time dependence of the exponents follows from a slight curvature of the lines. Both α and β increase with increasing quench depth ΔT_B. In Fig. 15 I_m is plotted versus Q_m in a double logarithmic scale. According to Eq. (19) the data follow a straight line whose slope gives β/α. In Fig. 16 the exponents β and β/α are plotted versus the quench depth ΔT_B. Contrary to α and β their ratio β/α is independent of the quench depth. Surprisingly, we get $d_f = \beta/\alpha = 2.43 \pm 0.05$, which is smaller than the expected value, namely, the Euclidean dimension $d = 3$, as predicted by Eq. (1). This observation will be further discussed later in the context of the scaling properties of $F(x)$. The sample thickness in these measurements was 10 μm. Results for a sample with a larger thickness of 100 μm are plotted in Fig. 16 (full symbols). The exponents for both samples agree very well. This demonstrates that our result is not influenced by the relatively small sample thickness or by wall effects. For different temperatures and sample thicknesses the values of the exponents d_f are summarized in Table III.

Quench-depth-dependent values for α and β were also found by Hashimoto *et al.* [42] for a high molecular mixture of PS/PVME with critical concentration, and by Takahashi *et al.* [18] for a noncritical mixture of PS/PPMS. On the other hand, Izumitani *et al.* [43] and both Nojima *et al.* [17] and Kuwahara *et al.* [19] got constant values of α and β for the high molecular SBR/PB [poly(styrene-r-butadiene) (SBR)/polybutadiene (PB)] and low molecular PS/PPMS.

D. Scaling of Q_m and I_m

$Q_m(t)$, $I_m(t)$, and t were transformed into dimensionless quantities $Q_m(t)$, $I_m(t)$, and t [Eq. (20)] to obtain the predicted master curve (see Sec. II E). For this purpose one needs the interdiffusion constant and the correlation length at

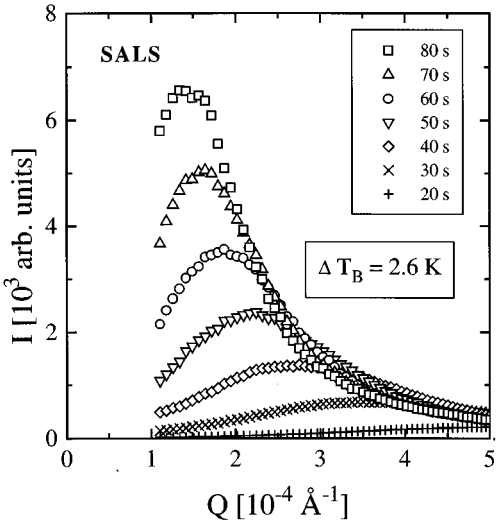

FIG. 11. Same as in Fig. 10 for the deepest quench $\Delta T_B = 2.6$ K. The scattering maximum is five times higher, passing the accessible Q window twenty times faster. As for the data in Fig. 10 the statistical error bars are always less than the size of the symbols.

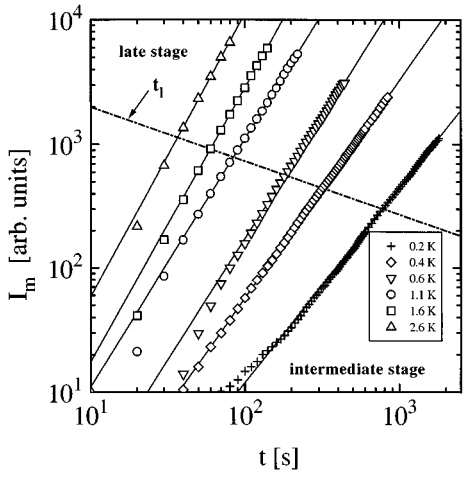

FIG. 13. Same plot as in Fig. 12 showing the intensity I_m vs time for different quench temperatures. The dashed line has the same meaning as in Fig. 12. I_m follows a simple power law.

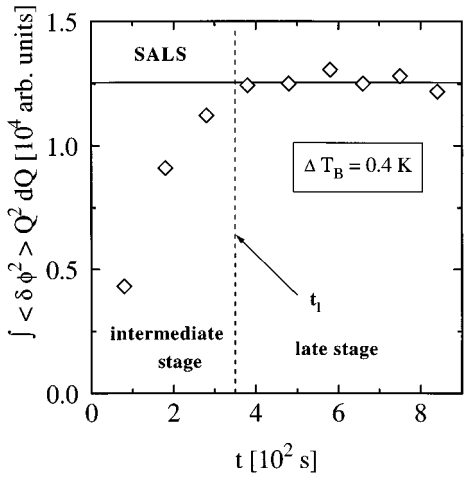

FIG. 14. Integral of the second moment of the order parameter depicted versus time, typical results for $\Delta T_B = 0.4$ K. The inset of a plateau marks the beginning of the late stage where the concentration difference of the domains reaches its value at the binodal.

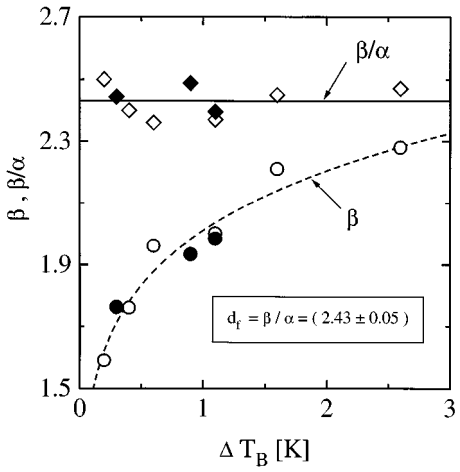

FIG. 16. Plot of the exponents β and β/α vs the quench depth ΔT_B. Summarizing Figs. 12, 13, and 15 the value of β depends on ΔT_B whereas the ratio β/α does not. Surprisingly, $d_f = \beta/\alpha = 2.43 \pm 0.05$ deviates from $d = 3$. Two sample thicknesses were used $x = 10\ \mu$m (open symbols) and $x = 100\ \mu$m (full symbols): The results are not influenced by wall effects.

the ''final'' temperatures of phase decomposition. Both quantities were found in the following way: (i) determination of the ''sample'' parameters ξ_+, D_0, and E_A from the measured ξ and D_c in the one-phase region with SANS and PCS. (ii) Extrapolation of ξ and D_c into the two-phase region using Eqs. (10) and (14). Thus the fit parameter to obtain the master curves for $Q_m(t)$ and $I_m(t)$ is the reduced temperature $\epsilon = (T_{S,\mathrm{expt}} - T_f)/T_f$ with the temperature after the quench T_f. Figure 17 shows that $Q_m(t)$ and $I_m(t)$ follow quite well a master curve. The fitted ϵ leads to $T_{S,\mathrm{expt}}$, it disagrees with the spinodal temperature obtained from extrapolation of $S^{-1}(0)$ (see Sec. II A) and is 0.2 K *above* the binodal temperature T_B. This implies that the kinetic experiments do not describe the results. Obviously, the interdiffusion constant in the gap between spinodal and binodal is already negative; i.e., phase separation takes place as if one were in the unstable regime. Under these circumstances, in the following the quenched steps will be characterized by $\Delta T_B \equiv (T_B - T_f)$ instead of $\Delta T_S \equiv (T_S - T_f)$.

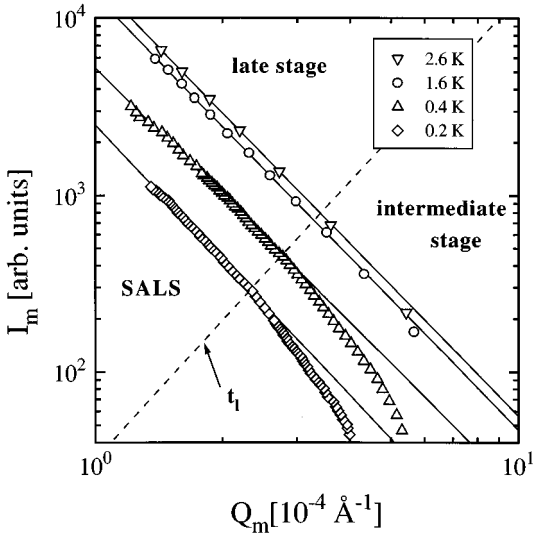

FIG. 15. Double logarithmic plot of I_m vs Q_m for various temperatures. Again a dashed line separates the intermediate from the late stage. Contrary to Figs. 12 and 13 the slopes of the straight lines fitted to the data in the late stage are now independent of the quench temperature.

In Fig. 18 several master curves are presented, as obtained for the same system PS/PPMS, but from different experiments together with theoretical predictions. The models of Langer-Bar-on-Miller (LBM) [44], Binder-Stauffer (BS) [16], and Siggia (S) [45] describe the phase separation only by a single process for all times. They reveal a constant slope for a limited part of our master curve. Furukawa's equation (F) [27] describes a wider time regime including different coarsening mechanisms; the results show a strong curvature. The master curve for our experimental data shows the same curvature as the theoretical curve by Furukawa. However, our data appear at reduced times smaller by nearly one order of magnitude. Experimental results of Nojima *et al.* (circles) [17] and Kuwahara *et al.* (triangles) [19] are also plotted in Fig. 18. Their data, on the other hand, appear at later reduced times than ours. We emphasize that Nojima *et al.* and Kuwahara *et al.* made their experiments at temperatures closer to the glass transition than we did. Furthermore, Kuwahara *et al.* used a scaling concept that differs from ours in Eq. (20). The reason for the observed discrepancy between our data and the theoretical prediction may result from the extrapolation of the diffusion constant D_c into a regime where the underlying Eq. (14) fails because of mode coupling effects. These tend to increase D_c [25]. Actually, a five times larger D_c would shift the experimental data in our master curve to larger reduced times, thus approaching the theoretical prediction.

E. Scaling of the structure factor at constant temperature

Figure 19 shows the scaled structure factor $F(x)$ (in arbitrary units) versus the scaled scattering vector x. It is plotted in a double logarithmic scale for different times in the late

TABLE III. Experimental nonequilibrium results of the *d*-PS/PPMS blend determined by SALS.

ΔT_B (K)	d (μm)	α	β	$d_f=\beta/\alpha$	t_l (s)	ΔT_S (K)	t_l^* (s)	η	n	$\langle l_l \rangle$ (10^3 Å)
0.2	10	0.62	1.59	2.50	750	0.4	700	4.88	2.14	6.8
0.3	100	0.72	1.76	2.44	550	0.5	520			
0.4	10	0.72	1.76	2.40	350	0.7	330	4.93	2.26	7.0
0.6	10	0.83	1.96	2.36	170	1.0	190	4.70	2.15	6.8
0.9	100	0.78	1.93	2.49	140	1.2	150			
1.1	10	0.83	1.98	2.37	90	1.4	90	4.56	2.38	6.8
1.1	100	0.83	2.00	2.39	100	1.4	90			
1.6	10	0.90	2.21	2.45	60	1.8	60	4.11	1.86	6.5
2.6	10	0.93	2.28	2.47	40	2.5	40	3.69	1.58	7.9

stage at $\Delta T_B=0.4$ K. In the range $x\leqslant 2$ where Q^{-1} is of the order of the domain size, the experimental data follow a master curve. The scaling hypothesis predicted by Eq. (1) is obeyed. However, the scaling leads to $d_f=2.43\pm0.05$, which we found for all quench depths studied. We emphasize that d_f agrees well with β/α obtained in the previous section. In Fig. 20 the region around the scattering maximum of $F(x)$ of Fig. 19 is expanded in scale and plotted linearly versus x [Fig. 20(a)]. For comparison, $F(x)$ is tentatively plotted for $d=3$ [Fig. 20(b)]. Obviously, the function does not scale. As already shown in Fig. 16 we emphasize that the unexpected value of d_f has nothing to do with the small sample thickness.

The validity of the dynamical scaling hypothesis for the late stage of phase separation demonstrates the evolution of self-similar structures. For compact structures scaling leads to the Euclidean dimension $d=3$. So far, no theoretical prediction exists that explains a value smaller than 3. However, the following considerations lead to a tentative interpretation. Combination of Eqs. (1) and (15) leads to

$$S(Q_m)\propto Q_m^{-3}\langle \delta\Phi^2\rangle. \tag{26}$$

For homogeneous or ''compact'' domains in the late stage one expects $S(Q_m)\propto Q_m^{-3}$; therefore $\langle \delta\Phi^2\rangle$ is constant and equal to $\Delta\Phi^2=(\Phi'-\Phi'')^2$. Since, from our results, $S(Q_m)\propto Q_m^{-2.43}$, it follows that $\langle \delta\Phi^2\rangle$ decreases with increasing time as $Q_m^{0.57}(t)$. This decrease of concentration difference cannot be attributed to strong thermal concentration fluctuations inside the domains. The PS-rich phase has a much larger viscosity than the PPMS-rich phase. Thus, we tentatively explain the decrease of the concentration difference by the buildup of PPMS-rich inclusions in the PS-rich domains. We assume that the PS-rich domains grow by coagulation. This leads to an increasing number of larger inclusions, which reduces $\langle \delta\Phi^2\rangle$ with increasing time. Under these circumstances the PS-rich phase has a noncompact structure, e.g., of ramified clusters [4], whose lifetime is larger than the time of investigation; i.e., the domains do not compactify during the observed coarsening. Obviously, the inclusions must have a broad distribution of sizes that must be larger than ξ and certainly smaller than $1/Q_m$.

We draw attention to other work, where a value of $d<3$ was observed. For the late stage of spinodal decomposition Nojima *et al.* [17] got $d_f=2.38\pm0.48$ for various off-critical

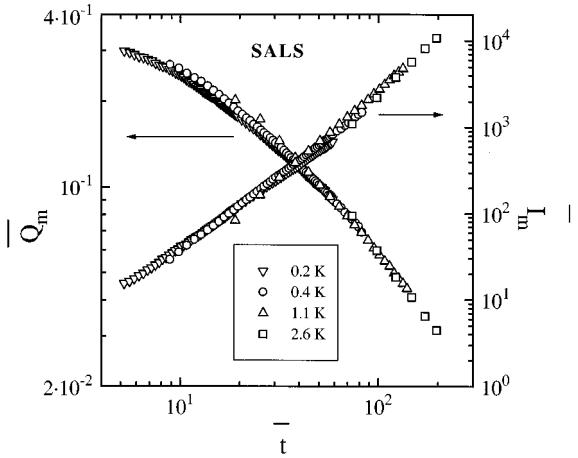

FIG. 17. Master curve for position and intensity of the scattering maximum as reduced quantities $\overline{Q}_m$ and $\overline{I}_m$, double logarithmically vs the reduced time $\overline{t}$.

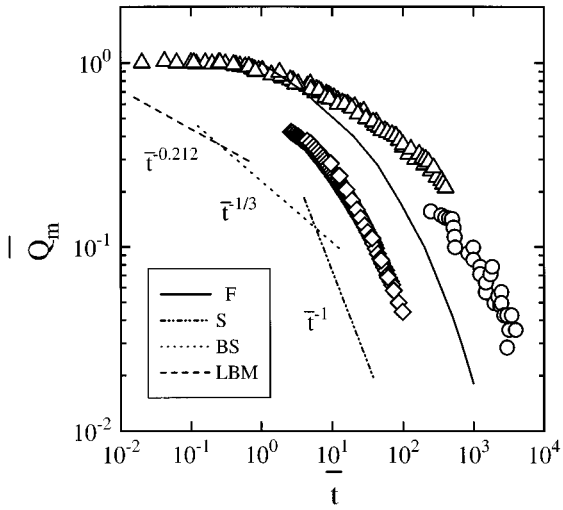

FIG. 18. Master curve of $\overline{Q_m}$ vs $\overline{t}$ obtained from different experiments and theories. The curvature of our master curve (diamonds) is in good agreement with Furukawa's theoretical prediction (full line), though lying at smaller reduced times. The results from Nojima *et al.* [17] (circles) and Kuwahara *et al.* [19] (triangles) are shifted in the opposite direction to larger reduced times. The straight lines of Siggia (dash-dotted line) [45], Binder and Stauffer (dotted line) [16], and Langer, Bar-on, and Miller (dashed line) [44] describe part of the master curve.

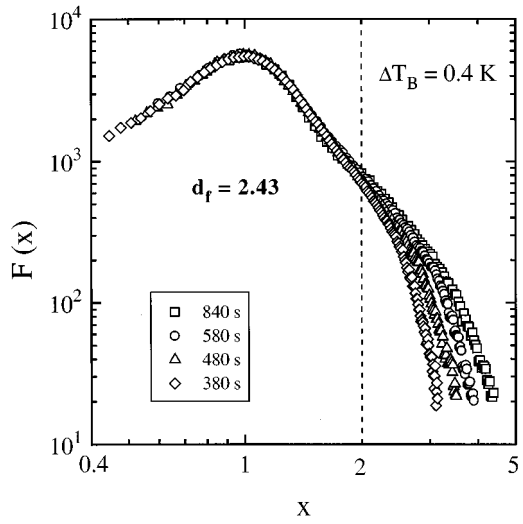

FIG. 19. Double logarithmic representation of the scaled structure factor $F(x)$ vs $x=Q/Q_m$ for different times in the late stage for $\Delta T_B=0.4$ K. Scaling was achieved for $x<2$ but with $d_f=2.43$ instead of $d=3$. For $x>2$ the curves do not scale.

mixtures, and $d_f=2.77\pm0.3$ for a critical mixture of PS/PPMS. In a more recent publication, these authors reported $d_f=2.6\pm0.4$ (off critical) and $d=3.0\pm0.2$ (critical) for the same blend but with a slightly different molecular weight [18]. On the other hand, Kuwahara *et al.* [19] found $d=3$ for the same system at critical concentration, and also a number of publications dealing with other polymer blends report a dimension $d=3$ for critical and noncritical concentrations as well.

A behavior with $d<3$ was found in previous experiments on the aggregation of a dense solution of latex spheres [46]. The agglomeration of the colloidal clusters shows spinodal type dynamics with a shifting scattering peak. Dynamical scaling was achieved for the later times of the aggregation process using $d_f=1.90\pm0.02$. In fact, the structure of these clusters exhibited a fractal morphology, and $d_f=1.90$ was also obtained from the slope of the structure factor versus Q in a double logarithmic plot. As stated before, our blend has a large viscosity difference between both components in the precipitated structure, i.e., the PS- and PPMS-rich phases have high and low viscosity, respectively. This is analogous to the latex system, where the colloidal particles are highly viscous or rigid and are embedded in a low viscous solvent.

For $x>2$ of Fig. 19 scaling for $F(x)$ fails, and $F(x)$ increases with time. According to Eqs. (21) and (23) the range $x>2$ is related to the ''local'' structure of the domain boundaries. The increase with time of the scaled structure factor means that the evolution of the interface structure has an inherent characteristic scale with a time dependence different from that of $1/Q_m$. As will be discussed below, a second length has to be introduced for a complete description. A second length scale was also found in the mixtures SBR/PB and PB/PI [polybutadiene (PB)/polyisoprene (PI)] as reported by Takenaka *et al.* [47,20], respectively.

Figure 21 shows two scaling functions $F(x)$ for times in the intermediate stage with $t\leqslant t_l$. One clearly sees that the scaling is not fulfilled at all. This is because $\langle\delta\Phi^2\rangle$ has not yet approached its equilibrium value. Table III compares the

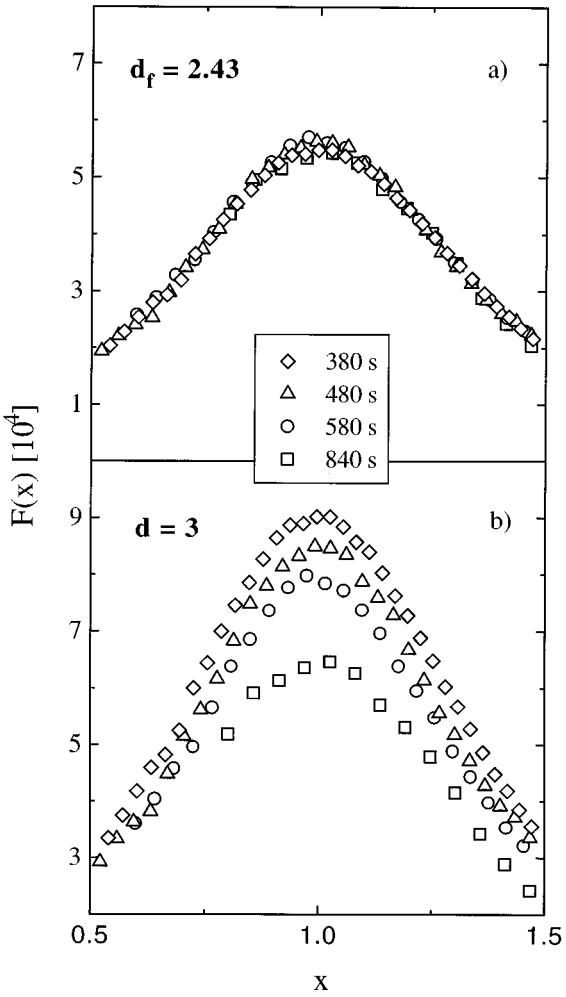

FIG. 20. (a) Linear representation of an expanded region around the maximum of $F(x)$ in Fig. 19. For direct comparison scaling with $d=3$ is plotted in (b). A common scaled structure factor can only be achieved with $d_f=2.43$.

values t_l^* for the determined transition time obtained with those found earlier from the inset of the plateau of the second moment in Fig. 14.

F. Scaling of the structure factor for different temperatures in the range $x\leqslant2$

So far we tested scaling of the domain structure in the range of $x\leqslant2$ during its time evolution at a fixed temperature. Now we test the dynamical scaling hypothesis of the structure factor. In order to compare its evolution for different temperatures it has to be normalized with $\langle\delta\Phi^2\rangle$ according to Eq. (15). To provide a comparison of all experimental scaling functions with the theoretical $\overline{F}(x)$ in Eq. (17) we normalize them to unity at $x=1$. The obtained structure factors are depicted in Fig. 22 for the different quenches. A nearly common curve is obtained for the four shallowest quenches. Quite generally, the curves slightly broaden for deeper quenches. The full lines represent the least-square fits for the theoretical scaling function Eq. (17). For the four shallowest quenches the mean curve from the theoretical fits were chosen for better representation. With deeper quench depth n decreases from 2.1 to 1.6 and η from 4.9 to 3.7. The

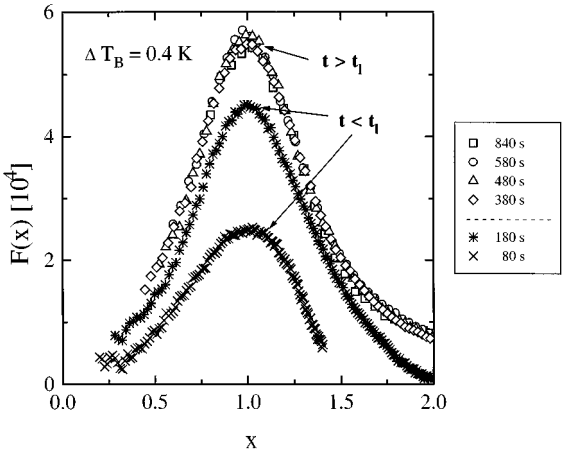

FIG. 21. $F(x)$ vs x for $\Delta T_B = 0.4$ K. As before a common curve was obtained for times $t > t_l$ in the late stage fulfilling the scaling hypothesis. Structure factors for times $t < t_l$ gave smaller $F(x)$, indicating that the order parameter is still growing in the range of the domain structure.

half-width Δx of the peak at Q_m increases from 0.8 to 1.1. The fit parameters are summarized in Table III. Contrary to our result recent publications reported $n = 4$ [21,26]. A value of $\eta = 6$ was found for various polymer systems of either critical or noncritical mixtures contrary to our results [18,19,42,43,47,48]. Only Nojima *et al.* [17] obtained $4.3 > \eta > 3.8$ for critical and noncritical mixtures of PS/PPMS, in good agreement with us.

With the exception of Takenaka and Hashimoto's work [20] a broadening of the peak in $F(x)$ is reported in various publications [48,49]. This is also in contrast to the theoretical work of Furukawa, which predicts a reduction of the peak width. Quite generally the phase separation at lower temperatures may be influenced by the finite quench rate. It was about 8 s for a step of $\Delta T_B \cong 1$ K. Thus, the temperature steps for the two deepest quenches possibly did not start from equilibrium.

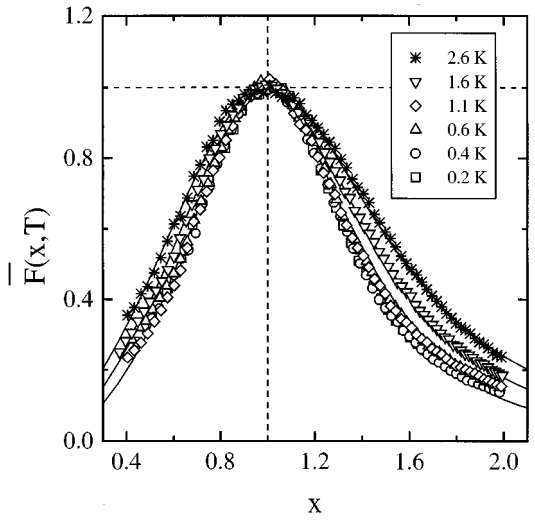

FIG. 22. Normalized scaled structure factors $\overline{F(x,T)}$ for different quench temperatures vs x. The full lines are Furukawa's theoretical predictions. The four shallow quenches lead to nearly the same scaling function which broadens for deeper quenches.

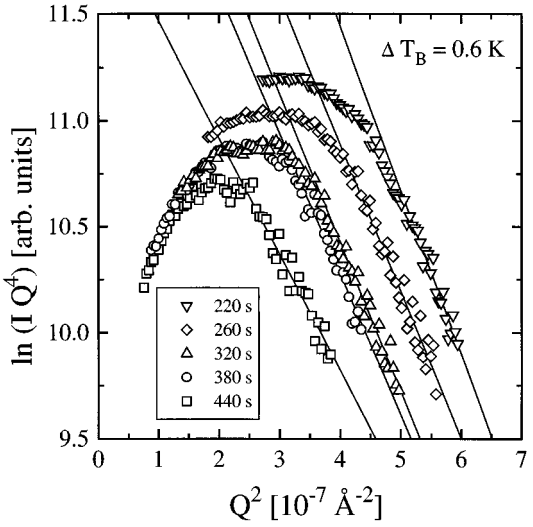

FIG. 23. Scattered intensity for different times at $\Delta T_B = 0.6$ K represented as $\ln(IQ^4)$ vs Q^2. For large Q values the data follow straight lines whose slope yields the interface thickness l_I as predicted by Eq. (21). A time dependence of the slope cannot be seen.

G. ''Local'' properties

In Fig. 19 the influence of ''local'' properties on the scattering function is observed in the range of large momentum transfers for $x \geq 2$. In Fig. 23 $\ln(IQ^4)$ is plotted versus Q^2 for various times at $\Delta T_B = 0.6$ K to analyze the scattered intensity following Eq. (21). At large Q the data can be fitted by straight lines, whose slope and ordinate values yield the interface thickness l_I and the Porod constant P, respectively. A time evolution of the interface thickness could not be seen. Thus, the mean values were taken from the results for all temperatures (Table III) and plotted versus the quench depth ΔT_B in Fig. 24. No relevant change of l_I is visible and the

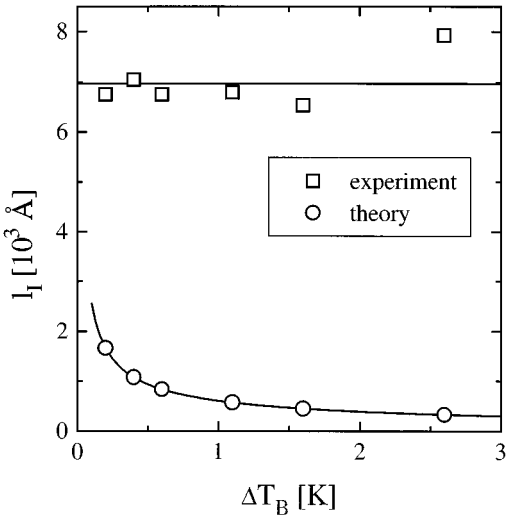

FIG. 24. Interface thickness l_I vs the quench depth ΔT_B. The experimentally obtained mean values for different times (squares) show no dependence from the quench temperature. Their mean value is plotted by the upper full line. This is in clear contradiction to the theoretical values calculated from Eq. (25), plotted as the lower full line. The experimental values are nearly one magnitude larger than the theoretical predictions.

mean value is plotted as a straight line. The theoretically predicted interface thickness should follow Eq. (22) with the previously obtained value of ξ_+ (see Sec. A), assuming 3D Ising behavior and the experimental values of ΔT_B. The resulting value is shown as a full line in Fig. 24 for comparison. The mean value for all times and temperatures gave $\langle l_I \rangle = 7000 \pm 200$ Å, nearly 2 orders of magnitude larger than the expected values $l_I = 2\sqrt{2}\xi$, which is of the order of 100 Å. This is an indication that the second characteristic length found for $x \geqslant 2$ is *not* the actual interface thickness. We assume that this high value follows from a waviness of the interface. Its amplitude is expected to be much smaller than $1/Q_m$ but larger than the correlation length ξ. Such a wavy interface leaves the relation $\beta = 3\alpha$ unchanged. An appreciable contribution of the ''true'' interface thickness to the domain size would lead to the relation $\beta > 3\alpha$, as experimentally confirmed by Bates and Wiltzius [26]. These authors introduced a so-called transition stage with a time regime having a non-negligible interface thickness. The observation $\beta > 3\alpha$ is in clear contradiction to our results; in our case the dynamical scaling remains valid though a second characteristic length is found.

Only few publications explicitly deal with the time evolution of the interfacial thickness. Takenaka and Hashimoto [20] observed an interface thickness decreasing with time and approaching a constant value, about four times larger than the theoretically expected value of Eq. (22).

V. SUMMARY AND CONCLUSIONS

In the binary polymer blend *d*-PS/PPMS of nearly critical concentration numerous temperature quenches were carried out into the two-phase regime with a quench depth $\Delta T_B \cong (T_B - T_f)$ from 0.2 to 2.6 K in order to study the phase separation with time-resolved SALS. For all our experiments the phase separation occurred in the metastable regime of the phase diagram because we had $\Delta T_B < (T_B - T_S)$. This was confirmed by SANS measurements, which probe the thermal concentration fluctuations in the one-phase region. The $3d$ Ising model is valid in the region where the quenches ended; i.e., thermal concentration fluctuations are strong. This was inferred from the crossover function [Eq. (11)], yielding $\mathrm{Gi} = 0.48 \pm 0.14$, which is much larger than for simple fluids. Our experiments observe homogeneous nucleation and growth, which are obviously induced by the strong thermal concentration fluctuations which initiate the phase separation with the formation of numerous clusters, which coarsen afterwards. This process has been proposed theoretically by Binder [22]. It is noteworthy that the amplitude of the concentration fluctuations is comparable with the order parameter itself, i.e., $\delta\Phi \cong \Delta\Phi$, and the spinodal loses its physical meaning. As a consequence of the strong thermal concentration fluctuations, the early stage of spinodal decomposition as described by the Cahn-Hilliard-Cook theory [12,13] does not appear at all. Surprisingly, the coarsening process of the domains in its late stage can still be described by the formalisms of spinodal decomposition if the spinodal temperature T_S is replaced by the binodal temperature T_B. Thus, for a quantitative description of the domain growth we used a quench depth $T_B - T_f$ instead of $T_S - T_f$. On the other hand, the equilibrium quantities, namely, the susceptibility $S(0)$ and the correlation length ξ diverge at the spinodal temperature T_S.

In all experiments, the scattered light intensity $I(Q,t,T)$ shows the typical maximum at a scattering vector $Q_m(t)$. The corresponding intensity $I_m(t)$ increases with time whereas Q_m shifts to smaller values. For the transition from the intermediate to the late stage of spinodal decomposition, the transition time t_l was determined by the inset of a plateau in the time-dependent second moment of the intensity [Eq. (16)]. During the late stage, both $Q_m(t)$ and $I_m(t)$ follow power laws in time with exponents α and β, respectively. The exponents depend on the quench depth. The ratio $\beta/\alpha = d_f$ was independent of the quench depth with $d_f = 2.43 \pm 0.05$. Surprisingly, this is smaller than the expected value $d = 3$. The structure factor $F(x)$ scales in the range $x = Q/Q_m < 2$ for all quench depths. This indicates the self-similar evolution of the precipitating structures. However, in Eq. (1) it was necessary to use $d_f = 2.43 \pm 0.05$ in agreement with the value obtained from β/α quoted before. The structure factor could be described by Furukawa's scaling function, which broadens for deeper quenches. The value of $d_f = 2.43$ is tentatively explained by a growing fraction of ''islands'' of the low viscous PPMS-rich phase embedded in the highly viscous PS-rich phase.

At larger Q, i.e., for $x > 2$, the scaling hypothesis fails also in the late stage. A second characteristic length was required for the description of the evolving structure. It is independent of time and quench depth, with $l_I = 7000 \pm 200$ Å. This value is much larger than the expected thickness $l_I = 2\sqrt{2}\xi$. We believe that this length is related to a waviness of the domain interface.

Furthermore, power laws hold for $Q_m(t)$ and $I_m(t)$ using the appropriate values for the interdiffusion coefficient and the correlation length in the two-phase region, respectively. Both were obtained from a fit of the reduced temperature with the equilibrium values of D_0, E_A, and ξ_+ determined by PCS and SANS in the one-phase region. The master curve of the scaled $\overline{Q_m(t)}$ has the same curvature as theoretically predicted, however, it is shifted towards smaller reduced times. This discrepancy may result from an incorrect extrapolation of the interdiffusion constant into a regime with strong mode coupling effects. A five times larger diffusion coefficient would give agreement between the experimental and theoretical data. The quench temperatures obtained from the fit are in good agreement with the experimental values if $\Delta T_B \equiv (T_B - T_f)$ was used.

From the PCS experiments at higher temperatures an extra slow relaxation process in the 0.1-s region was observed and related to density fluctuations.

ACKNOWLEDGMENTS

The authors acknowledge Professor E. W. Fischer (MPI-Polymer-Research, Mainz) for the use of the light scattering spectrometers, Dr. Th. Wagner (MPI-Polymer-Research, Mainz) for the preparation of the PPMS component, Professor K. Mortensen (Risø National Laboratory, Denmark) for his help during the SANS experiments, and Professor K. Binder (University Mainz) and Professor P. Fratzl (University Vienna) for helpful discussions.

[1] P. G. de Gennes, *Scaling Concepts in Polymer Physics* (Cornell University, Ithaca, 1979).
[2] J. D. Gunton, M. San-Miguel, and P. S. Sahni, *Phase Transitions and Critical Phenomena* (Academic, New York, 1983), Vol. 8.
[3] T. Hashimoto, *Materials Science and Technology, Vol. 12, Structure and Properties of Polymers* (VCH, Weinheim, 1993).
[4] K. Binder, *Advances in Polymer Science* (Springer-Verlag, Berlin, 1994), Vol. 112, pp. 181–299.
[5] Herkt-Maetzky and J. Schelten, Phys. Rev. Lett. **51**, 896 (1983).
[6] D. Schwahn, K. Mortensen, and H. Yee-Madeira, Phys. Rev. Lett. **58**, 1544 (1987).
[7] F. S. Bates, J. Rosedale, P. Stepanek, T. P. Lodge, P. Wiltzius, G. H. Fredrickson, and R. P. Hjelm, Phys. Rev. Lett. **65**, 1893 (1990).
[8] M. Y. Belyakov and S. B. Kiselev, Physica A **190**, 75 (1992).
[9] P. G. de Gennes, J. Phys. (Paris) Lett. **38**, L441 (1977).
[10] J. v. Sengers, in *Supercritical Fluids*, edited by E. Kiran and J. M. H. Levelt Sengers (Kluwer Academic Publishers, Dordrecht, 1994), pp. 231–271.
[11] D. Schwahn, G. Meier, K. Mortensen, and S. Janssen, J. Phys. (France) II **4**, 837 (1994).
[12] J. W. Cahn, Acta Metall. **9**, 795 (1961).
[13] H. E. Cook, Acta Metall. **18**, 297 (1970).
[14] D. Schwahn, S. Janssen, and T. Springer, J. Chem. Phys. **97**, 8775 (1992).
[15] G. Müller, D. Schwahn, H. Eckerlebe, J. Rieger, and T. Springer, J. Chem. Phys. **104**, 5326 (1996).
[16] K. Binder and P. Stauffer, Phys. Rev. Lett. **33**, 1006 (1974).
[17] S. Nojima, K. Tsutsumi, and T. Nose, Polym. J. **14**, 225 (1982); **14**, 907 (1982).
[18] M. Takahashi, H. Horiuchi, S. Kinoshita, Y. Ohyama, and T. Nose, J. Phys. Soc. Jpn. **55**, 2687 (1986).
[19] N. Kuwahara, H. Sato, and K. Kubota, Phys. Rev. E **47**, 1132 (1993).
[20] M. Takenaka and T. Hashimoto, J. Chem. Phys. **96**, 6177 (1992).
[21] J. F. Joanny and L. Leibler, J. Phys. (Paris) **39**, 951 (1978).
[22] K. Binder, Phys, Rev. A **29**, 341 (1984).
[23] H. Swinney and D. Henry, Phys. Rev. A **8**, 2586 (1973).
[24] L. v. Hove, Phys. Rev. **95**, 1374 (1954).
[25] G. Meier, B. Momper, and E. W. Fischer, J. Chem. Phys. **97**, 5884 (1992).
[26] F. S. Bates and P. Wiltzius, J. Chem. Phys. **91**, 3258 (1989).
[27] H. Furukawa, Adv. Phys. **34**, 703 (1985).
[28] C. Yeung, Phys. Rev. Lett. **61**, 1135 (1988).
[29] H. Furukawa, Phys. Rev. B **40**, 2341 (1989).
[30] Y. C. Chou and W. I. Goldburg, Phys. Rev. A **20**, 2015 (1979).
[31] M. G. Brereton, E. W. Fischer, G. Fytas, and U. Murschall, J. Chem. Phys. **86**, 5174 (1987).
[32] G. Müller and T. Springer, Rev. Sci. Instrum. (to be published).
[33] R. S. Stein and J. J. Keane, J. Polym. Sci. **17**, 21 (1955).
[34] D. Schwahn, K. Mortensen, and S. Janssen, Phys. Rev. Lett. **73**, 1452 (1994).
[35] D. Schwahn, H. Eckerlebe, E. Hädicke, and T. Springer, J. Phys. (France) I **3**, 13 (1993).
[36] E. W. Fischer, Physica A **201**, 183 (1993).
[37] D. W. Hair, E. K. Hobbie, J. Douglas, and C. C. Han, Phys. Rev. Lett. **68**, 2476 (1992).
[38] G. Meier, D. Vlassopolous, and G. Fytas, Europhys. Lett. **30**, 325 (1995).
[39] T. Schmackers and D. Schwahn, Macromolecules (to be published).
[40] Additionally the phase separation temperatures depend on the sample thickness in the range under consideration [41], e.g., we found $T_B = (118.1 \pm 0.1)$ °C for the larger sample thickness $x_s = 100$ μm.
[41] S. Reich and Y. Cohen, J. Polym. Sci. **19**, 1255 (1981).
[42] T. Hashimoto, M. Itakura, and N. Shimidzu, J. Chem. Phys. **85**, 6773 (1986).
[43] T. Izumitani, M. Takenaka, and T. Hashimoto, J. Chem. Phys. **92**, 3213 (1990).
[44] J. S. Langer, M. Bar-on, and H. D. Miller, Phys. Rev A **11**, 1417 (1975).
[45] E. D. Siggia, Phys. Rev. A **20**, 595 (1979).
[46] M. Carpineti and M. Giglio, Phys. Rev. Lett. **68**, 3327 (1992).
[47] M. Takenaka, T. Izumitani, and T. Hashimoto, J. Chem. Phys. **92**, 4566 (1990).
[48] P. E. Tomlins and J. S. Higgins, J. Chem. Phys. **90**, 6691 (1989).
[49] T. Hashimoto, M. Itakura, and H. Hasegawa, J. Chem. Phys. **85**, 6118 (1986).